ARTICLE OPEN

Check for updates

Corrosion behavior of pure Ti under continuous NaCl solution spraying at 600 °C

Rui Li[1], Li Liu[1]✉, Yu Cui[2], Rui Liu[1] and Fuhui Wang[1]

The corrosion behavior of pure Ti under continuous NaCl solution spraying at 600 °C, compared with that under solid NaCl deposit film in $H_2O + O_2$ environment, has been studied by mass gain curves, detailed microstructural investigation and phase-stability diagram. The results indicate that the oxide scale consists of three repeated multi-layered subscales composed of Na_2TiO_3 and TiO_2. Continuous NaCl increases the volatilization of $TiCl_4$ towards oxide/atmosphere interface as well as introduces pores and cracks. Pores and cracks allow the oxidizing atmosphere to enter and rapidly spread and resulting in a repeat multi-layered oxide scale. Relatively dense repeat TiO_2 delayed active oxidation process, which will decrease the corrosion rate of the pure Ti under NaCl spraying.

npj Materials Degradation (2022)6:53 ; https://doi.org/10.1038/s41529-022-00257-x

INTRODUCTION

Compared with the inland areas, the marine environment is more corrosive, which is mainly due to marine air containing abundant salts and water vapor. The corrosion behavior of compressor blades working in the marine environment had been accelerated by the synergistic effect of solid NaCl deposits and water vapor at 300–600 °C[1–4]. Many authors have been dedicated to studying the corrosion behavior of 1Cr11Ni2W2MoV[5], pure Cr[6], Fe-Cr alloys[7], and Ni-based alloys[8,9] used in compressor blade materials under a solid NaCl deposit film at 500–700 °C, whether water vapor is present or not. The results show that these materials suffer active oxidation. The oxide scale was very cracked and porous. Active oxidation is a cyclic process, chlorine is proposed to be formed at the sample surface and then penetrate the oxide scale to form volatile transition metal chlorides at the scale/metal interface. Because of the high vapor pressure of the metal chlorides they will then diffuse outwards through the scale and decompose into a porous metal oxide and chlorine closer to the scale surface. The released chlorine is proposed to partly diffuse back to the scale/metal interface and continue the oxidation process without self-consumption acting like a corrosion catalyst, accelerating corrosion[1]. In addition, electrochemical reactions may occur during the corrosion process[10–14].

Ti-based alloys have been widely used in the compressor components of aero-engine gas turbine materials for their excellent physical and mechanical properties at elevated temperature[15–17]. The oxidation of Ti alloys under solid deposit NaCl film at 500–600 °C also have been investigated, Fan et al.[18,19] studied the corrosion behavior of Ti60 alloy under precoated solid NaCl deposit film (4 mg cm^{-2}) in H_2O and O_2 (30.8 vol.% H_2O, O_2: 140 mL min^{-1}) at 600 °C, the oxide scale was layered, the outer layer consisted of $Na_4Ti_5O_{12}$ and TiO_2, while the inner layer with lamellar structure included alloying elements oxides (Al_2O_3, SnO_2, ZrO_2, and titanium oxide with low valence). Ciszak et al.[20–22] studied the corrosion behavior of Ti alloys under precoated solid NaCl deposit (3-4 mg cm^{-2}) under dry and moist air (12 vol.% H_2O, air steam: 8 mL min^{-1}) at 560 °C, the degradation of these Ti alloys in this environment mainly due to "active oxidation" mechanism[23–26].

In fact, the solid NaCl deposit environment is a type of acceleration laboratory method with a thick NaCl deposit layer, low oxygen, and low H_2O steam. The experimental condition closer to the actual service environment is a continuous NaCl solution spraying simulation condition with ununiform NaCl deposit, rich oxygen, and rich H_2O steam. The corrosion behavior of Fe-20Cr in NaCl solution spraying at 600 °C was investigated in ref. [1]. NaCl solution spraying destroyed the protective Cr_2O_3 scale, forming a Na_2CrO_4 and $FeCr_2O_4$ inner layer and a defective columnar crystal Fe_2O_3 outer layer. However, the corrosion reactions of pure Ti in the continuous NaCl solution spraying environment are not clear at present.

The aim of the present work is to better understand the corrosion behavior of pure Ti under NaCl solution spray at 600 °C, compared with that of under solid NaCl deposit in water vapor at the same temperature. Detailed microstructural investigation of the base corrosion products at different times in combination with the phase stability diagram to explain the corrosion mechanism of pure Ti.

RESULTS

Corrosion kinetics

Figure 1 shows the corrosion kinetics of a pure Ti during the testing time of 20 h under three conditions at 600 °C, which are as follows: mass gain without NaCl < mass gain with continuous NaCl solution spraying < mass gain with solid NaCl deposit film in $H_2O + O_2$.

The mass gain increase follows parabolic curves after 20 h corrosion for three conditions at 600 °C. The parabolic rate constants, k_p, for the period of parabolic growth are 9.48×10^{-13} g^2 cm^{-4} s^{-1}, 1.71×10^{-11} g^2 cm^{-4} s^{-1}, and 5.52×10^{-10} g^2 cm^{-4} s^{-1} obtained without NaCl, under continuous NaCl solution spraying and under solid NaCl deposit film in $H_2O + O_2$

[1]Shenyang National Laboratory for Materials Science, Northeastern University, 110819 Shenyang, China. [2]Shi-changxu Innovation Center for Advanced Materials, Institute of Metal Research, Chinese Academy of Sciences, 110016 Shenyang, China. ✉email: liuli@mail.neu.edu.cn

environment, respectively, according to Eq. (1):

$$\left(\frac{\Delta m}{S}\right)^2 = 2k_p t \quad (1)$$

where $\frac{\Delta m}{S}$ is the mass gain per unit surface area in g cm^{-2}, t is time in s, and k_p is the parabolic rate constant in g^2 cm^{-4} s^{-1}.

The total mass gain of the pure Ti in continuous NaCl solution spraying at 600 °C for 20 h is near 1.57 mg cm^{-2}. The mass gain of the pure Ti under the solid NaCl deposit film after 20 h in $H_2O + O_2$ is near 8.92 mg cm^{-2}, which is approximately 6 times more than that exposed to continuous NaCl solution spraying. This result shows that the corrosion mechanisms of pure Ti under continuous NaCl solution spraying and solid NaCl deposit film in $H_2O + O_2$ environment at 600 °C are different from each other.

Chemical compositions of corrosion products

The corrosion products of samples exposed to continuous NaCl solution spraying at 600 °C for 5 and 20 h were detected by XRD (see Fig. 2). Figure 2a shows GAXRD patterns of the inner layer corrosion layer neared the based metal that consists mainly of TiO_2. Figure 2b shows XRD patterns of the outer layer corrosion layer scratched from the samples, mixed oxides that consist mainly of TiO_2 and Na_2TiO_3 form on the alloy surface at all times, and residual NaCl is also detected after 20 h.

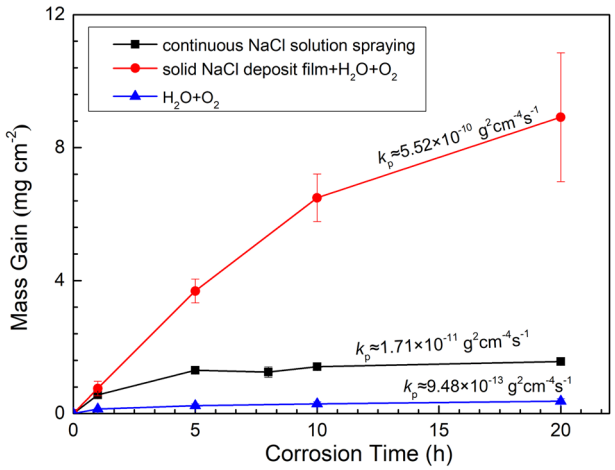

Fig. 1 Mass gain curves of Ti exposed to different environments for 20 h at 600 °C. Continuous NaCl solution spraying (—■—), solid NaCl deposit film+H_2O+O_2 (—●—), H_2O+O_2 (—▲—). Error bars represent standard deviations.

Surface and cross-sectional morphologies

Figure 3 shows the surface morphologies of the pure Ti samples after corrosion under continuous NaCl solution spraying at 600 °C for 30 s, 2 min, 1 h, 5 h, 10 h, and 20 h. As shown in Fig. 3a, after 30 s, NaCl particles with the regular tetrahedral structure were deposited on the sample surface, and at this time oxidation occurs indistinctly. As shown in Fig. 3b, after 2 min, the oxidation particles formed uniformly, and the NaCl particles change to be wrinkled. After 1 h, the surface morphology in Fig. 3c shows that there are two kinds of deposit NaCl particles: one is NaCl particles with concave–convex folds on the surface, and the other is NaCl particles with smooth surfaces and boundaries. Considering that smooth NaCl particles are deposited on gully NaCl particles, it is thought that the smooth NaCl particles are freshly deposited, while the rugged NaCl particles should be already reacted with oxides. Currently, the amount of deposited NaCl particles is more than that at the initial time. In addition, the oxides are very uniform, and small white particles are formed. The surface morphologies of pure Ti after corrosion 5 h in Fig. 3d, e show that NaCl particles with local reaction appeared. In order to confirm the universality of this phenomenon, the same phenomenon was found on several samples at the same time node, as shown in Fig. 3d, e. The common results are that: (1) the corrosion products are no longer uniform, some of them are needle-like, some of them are white raised, and there are fresh small NaCl particles deposited; (2) the deposited NaCl particles with smooth boundaries have local reaction zones, which should be formation by NaCl reacting with Ti oxides. After 10 h (in Fig. 3f), the oxides are needle-like structures and there are NaCl particles deposited. After 20 h (in Fig. 3g), the needle-like oxides covered the sample surface and look compact, NaCl mixed with needle-like oxides can be observed in the local area. This is different from the surface morphologies of samples after corrosion for 20 h under the solid NaCl deposit film in $H_2O + O_2$, which is porous and defective[3,4]. Considering that these morphologies have been reported in detail, they are not shown repeatedly.

Figure 4 shows the cross-sectional morphologies of pure Ti samples after corrosion under continuous NaCl solution spraying at 600 °C for 5 h and 20 h. Figure 4a shows that the whole corrosion scale on pure Ti is approximately 5 μm thick after corrosion 5 h. The corrosion product seems to have two layers structure. The inner layer next to the substrate is white, and the thickness is very thin; the outer layer is slightly darker, and there

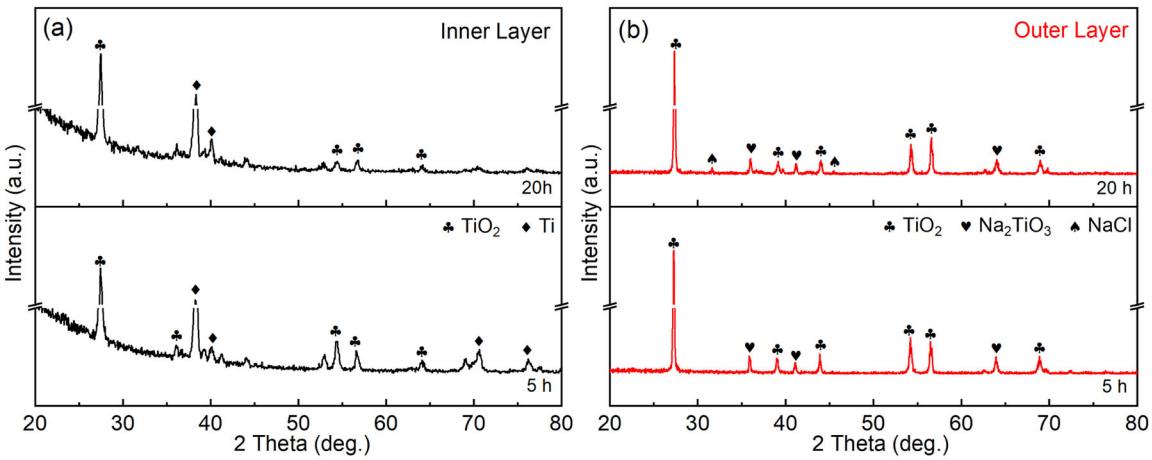

Fig. 2 XRD patterns of the corrosion products of the Ti after corrosion with continuous NaCl solution spraying for 5 h and 20 h at 600 °C. **a** the corrosion products of the inner layer, and **b** the corrosion products of the outer layer.

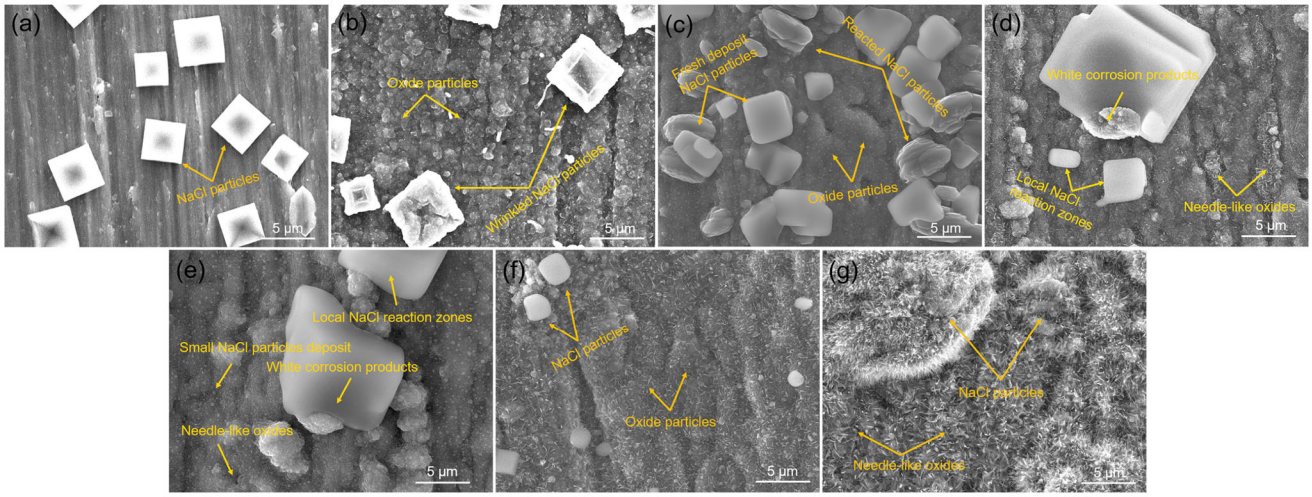

Fig. 3 SEM surface morphologies of samples exposed to the continuous NaCl solution spraying for different times at 600 °C. a 30 s, **b** 2 min, **c** 1 h, **d**, **e** 5 h, **f** 10 h, and **g** 20 h.

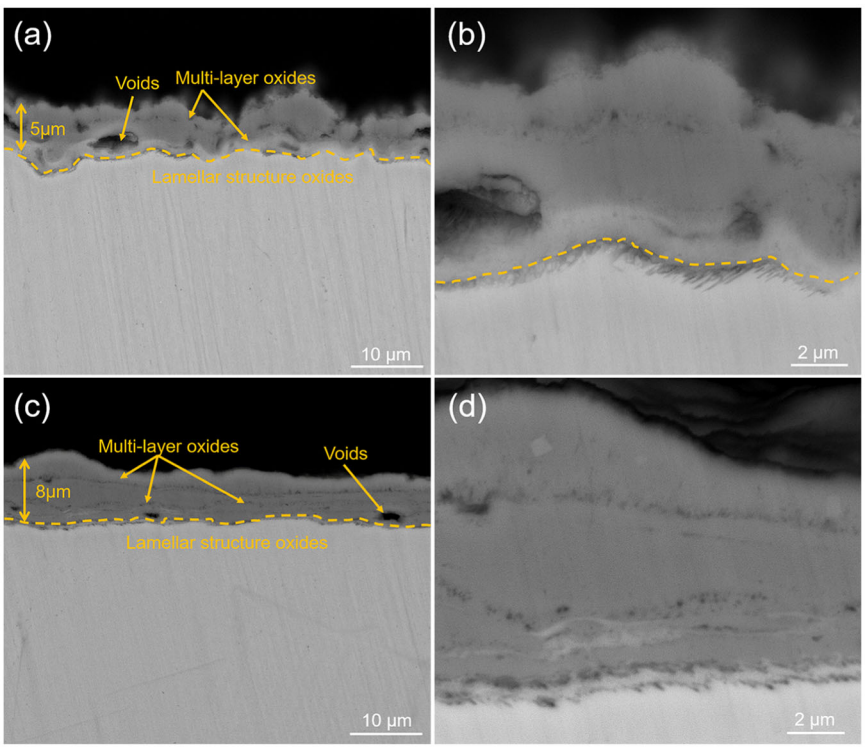

Fig. 4 SEM cross-section morphologies and an enlarged picture of samples exposed to the continuous NaCl solution spraying for different times at 600 °C. a b 5 h and **c d** 20 h.

are a lot of defects inside. Another interesting result is that there are filamentous or lamellar-like corrosion products at the interface between corrosion products and matrix, seeing enlarged results in Fig. 4b. This kind of oxide has been also found in the studies of both Ti60 alloy[19] and Ti-6Al-2Sn-4Zr-2Mo-Si alloy[22] under solid NaCl deposit film in $H_2O + O_2$ environment, but it is found by TEM and not so obvious as this. After 20 h, the thickness of the corrosion scale layer is about 8 μm, and the corrosion scale layer is a multilayer structure through continuous defects segmentation, as shown in Fig. 4c. There are still large-scale defects in the corrosion product scale. At the oxide/metal interface, there are also filamentous corrosion products and a white corrosion product layer, as shown in Fig. 4d. The corrosion products formed under solid NaCl deposit film in $H_2O + O_2$ with total thicknesses of approximately 65 μm[3,4].

Cross-sectional microstructure by TEM

The cross-sectional TEM samples of corrosion for 5 h and 20 h have been prepared by FIB. The cross-sectional microstructure and compositions of the corrosion products were determined by TEM. Supplementary Fig. 1a shows the surface morphology of the sample after corrosion for 5 h in SEM backscattered electron (BSE). NaCl particles show a darker color than corrosion oxides. some of the NaCl particles in the center part formed corrosion products. In order to study the information of corrosion products formed in the

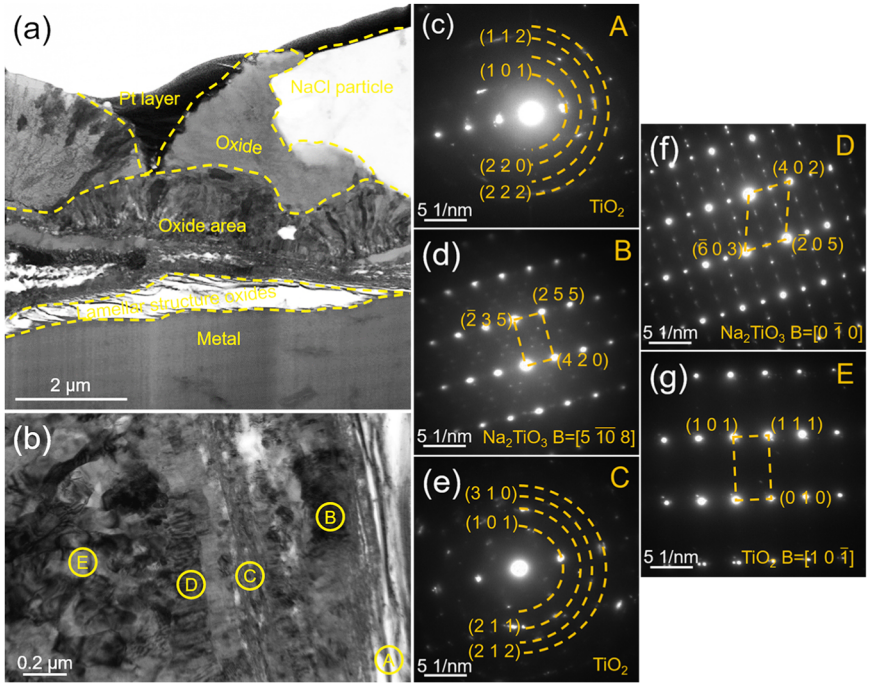

Fig. 5 TEM results of Ti exposed to the continuous NaCl solution spraying for 5 h at 600 °C. a STEM cross-section morphology, **b** inner layer TEM enlarged view, **c** SAED patterns of area A, **d** SAED patterns of area B, **e** SAED patterns of area C, **f** SAED patterns of area D, and **g** SAED patterns of area E.

coexistence state with NaCl particle, FIB milled areas were along the reaction zone of oxide and NaCl particle. Supplementary Fig. 1b shows a FIB-milled cross-section of the sample. Pt-layer is used to protect the surface of the selected area of interest including the NaCl particle.

Figure 5a shows the STEM bright-field image of FIB milled sample. A large number of cracks, defects, and pores are in the corrosion products, especially at the oxide/metal interface. Filiform corrosion products are formed near the base metal, as shown in Fig. 4a. In addition, the corrosion products formed near NaCl particle are different from the oxides in other parts. From the metal matrix to the NaCl particle (marked A to F region), the structure and composition of corrosion products were carefully analyzed by TEM. Figure 5b shows the enlarged image of the selected area in Fig. 5a, which includes A–E region from the adjacent substrate to the outer layer. The filiform corrosion product closed to base metal (marked A region) looks like the lamellar structure Ti_2O oxides or TiO_2 oxides formed in the inner layer of corrosion products on Ti60 alloy[18,19] or other Ti alloys[20,22] under solid NaCl deposit film in $H_2O + O_2$ environment at about 600 °C. The results of the selected area electron diffraction pattern (SAED) confirm that the main product in A region should be TiO_2, as shown in Fig. 5c. In Fig. 5b, the morphology of B region shows no obvious crystal structure and is different from A region. By selected area electron diffraction, the corrosion products in B region were identified as Na_2TiO_3, shown in Fig. 5d. The outer layer C region shows a strip structure, and the corrosion products are identified as TiO_2 in Fig. 5e. The D region in Fig. 5b shows no longer a strip structure, and the corresponding corrosion products are Na_2TiO_3 as shown in Fig. 5f. The E region in Fig. 5b corresponding corrosion products are TiO_2 as shown in Fig. 5g. The marked F region is near to NaCl particle in Fig. 5a, which shows different color and structure from other corrosion products. Figure 6a shows the enlarged image of the F region in Fig. 5a, and the next selected area electron diffraction analysis in Fig. 6b and corresponding EDS results in Fig. 6c reveal that the corrosion products in F region is Na_2TiO_3. The scale consisted of three duplicated and multi-layered oxide subscales with a total thickness of about 5 μm.

Supplementary Fig. 2 shows the surface morphology of the sample after corrosion 20 h in SEM BSE mode. In order to study the propagation stage of the NaCl-induced corrosion attack, FIB milled areas were across the needle-like oxides, as shown in Supplementary Fig. 2a. Supplementary Fig. 2b shows a FIB-milled cross-section of the sample. There are obvious cracks in the corrosion products, especially at the oxide/metal interface. These results are similar to the results for corrosion 5 h.

Figure 7a shows the STEM bright-field image of FIB milled sample. The oxide scale consisted of several delamination layers which are often cracks, defects, and pores and have partly detached from each other by layered small pores and columnar voids that parallel to the oxide/metal interface. From the metal matrix to the NaCl particle (marked G to I region), the structure and composition of corrosion products were carefully analyzed by TEM. Figure 7b shows the enlarged image of the selected area in Fig. 7a, which included the area from the adjacent substrate to the outer layer. the general microstructure of the inner filiform corrosion product close to the base alloy (corresponding to the circled area G) looks like the lamellar structure Ti_2O oxides or TiO_2 oxides formed after 5 h corrosion. The oxides have very fine grains consisting mostly of TiO_2 oxide as confirmed by SAED of one of the oxide grains. An example of a result identified as TiO_2 in [0 −1 1] orientation is shown in Fig. 7c. The outer layer in Fig. 7b, the morphology of H region shows a strip structure similar to E region. By SAED, the corrosion products in H region were also identified as TiO_2 in [−1 0 1] orientation, shown in Fig. 7d. The outer layer I region shows a strip structure, and the corrosion products are identified as Na_2TiO_3 in Fig. 7e.

Cross-sectional elemental distribution by EPMA

The elemental distribution of corrosion products in the cross-section was studied by EPMA. Figure 8 shows the EPMA results of corrosion products of pure Ti formed after corrosion for 5 and 20 h in continuous NaCl solution spraying at 600 °C, which include mainly the participating elements Ti, Na, O, and Cl. Figure 8a

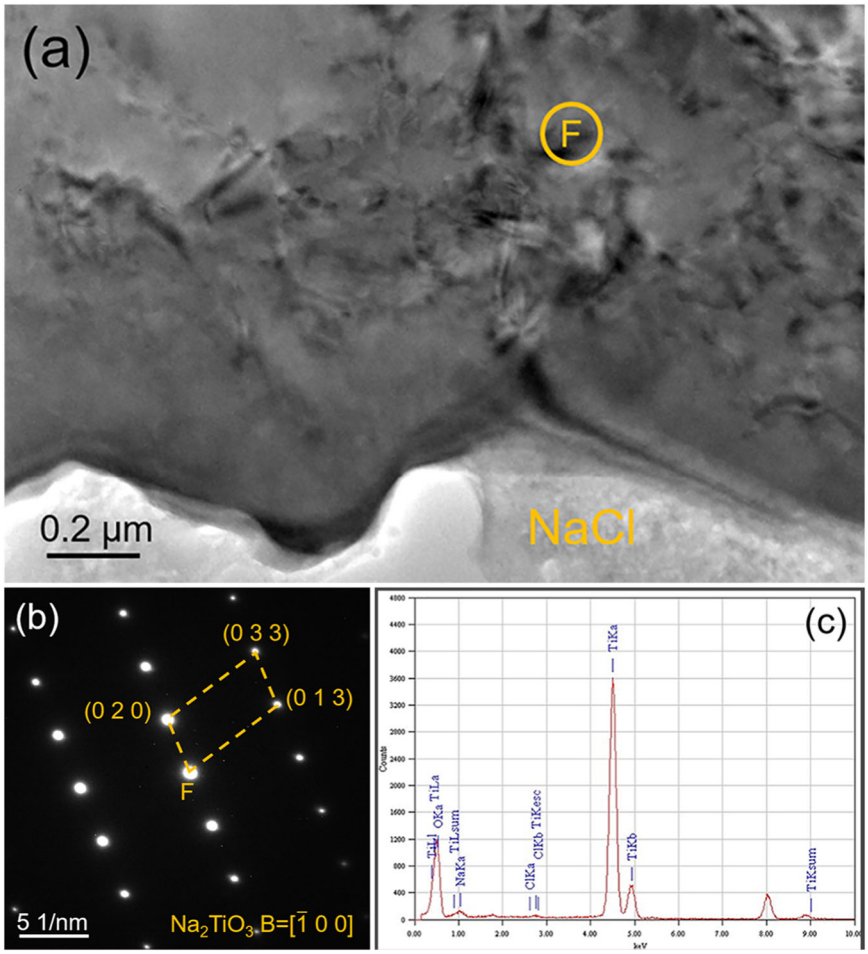

Fig. 6 Outer layer TEM results of pure Ti after corrosion in continuous NaCl solution spraying for 5 h at 600 °C. a TEM image, **b** SAED patterns of area F, and **c** the EDS spectra of area F.

shows the EPMA after 5 h, which shows that Ti and O is present throughout the oxides. Cl is mainly in the inner layer near the based metal; Na is full in the outer layer. From the EPMA results of 20 h (Fig. 8b), Ti and O occur throughout both layers, Na is distributed in the layer, and the distribution of Na is more concentrated in the surface layer. Cl is still in the inner layer near to based metal.

DISCUSSION

Previous studies on pure Ti[3,4] have shown higher NaCl environment promotes the growth of Ti oxides and increases the active oxidation rate under solid NaCl deposit film in $H_2O + O_2$ at 600 °C. Nevertheless, the microstructure and the composition of the corrosion scales growing on pure Ti in the presence of continuous NaCl solution have not been investigated in detail and the corrosion mechanism are still under debate. The present study focuses on the influence of the continuous NaCl solution environment on corrosion of pure Ti at 600 °C, compared with that under a solid NaCl deposit+$H_2O + O_2$ environment. This study includes a detailed TEM microstructural investigation of the corrosion products at different times in combination with the phase stability diagram.

The present study indicated that the presence of continuous NaCl solution influenced and accelerated the corrosion process of the oxide scale formed on pure Ti at 600 °C. The mass gain per unit area was 4 times than that for $H_2O + O_2$, but less than for a solid NaCl deposit film environment. Several studies reported this detrimental effect of NaCl deposit on the oxidation resistance of pure Ti and Ti-alloys[3,4,18–22,27,28]. It was related to the initial reaction of native TiO_2 with NaCl releasing Cl_2, which initiates an active oxidation mechanism and increases the corrosion rate in presence of NaCl deposit.

The overall corrosion process and mechanism of pure Ti under continuous NaCl solution spraying at 600 °C has been studied based on the above experimental data. Under a continuous NaCl solution spraying environment, only a small amount of NaCl was deposited on the surface of the sample, sufficient O_2 and H_2O from the environment reacted with Ti, see Fig. 3a, b, TiO_2 formed on the sample surface[29–32]. This result was consistent with theoretical predominance diagrams of Na-Ti-O-Cl-H shown in Fig. 8. It shows that the atmospheres with high O_2 partial pressure in the NaCl solution-spraying experiments explicitly favored the formation of TiO_2 instead of $TiCl_x$ (s, g), that is, the oxides were thermodynamically stable species.

And then NaCl was consumed and fresh NaCl particles were deposited on the sample surface at the same time. The degree of corrosion depended on the thermodynamic properties and distribution of NaCl particles. As shown in Fig. 3d, e, the rapidity of the corrosion attack, especially in the vicinity of NaCl particles was a prominent feature of this study, NaCl particles began to react with oxide. This was in accordance with Jonsson's work[33], which studied the initial oxidation of Fe-2.25Cr-1Mo in the presence of small amounts of KCl through ESEM at 400 °C. It was concluded that the corrosion occurred around KCl particles, the KCl particles completely react with oxide and KCl particles

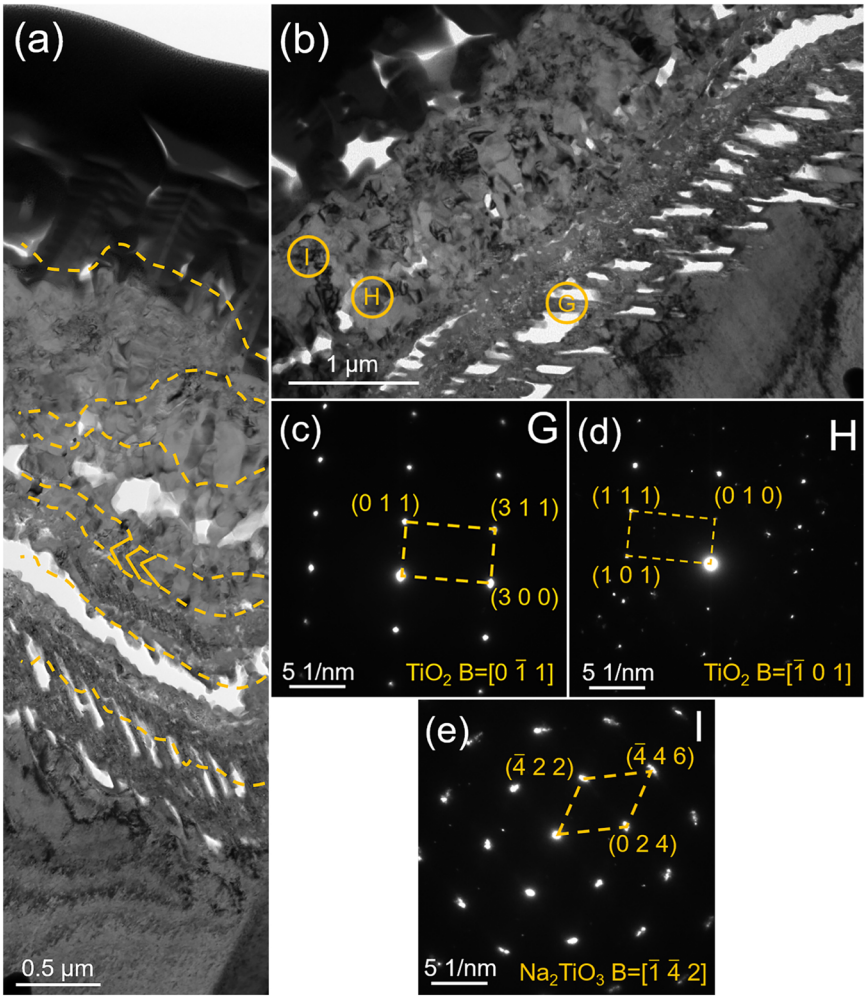

Fig. 7 TEM results of Ti exposed to the continuous NaCl solution spraying for 20 h at 600 °C. a STEM bright field image, **b** the TEM enlarged view, **c** SAED patterns of area G, **d** SAED patterns of area H, and **e** SAED patterns of area I.

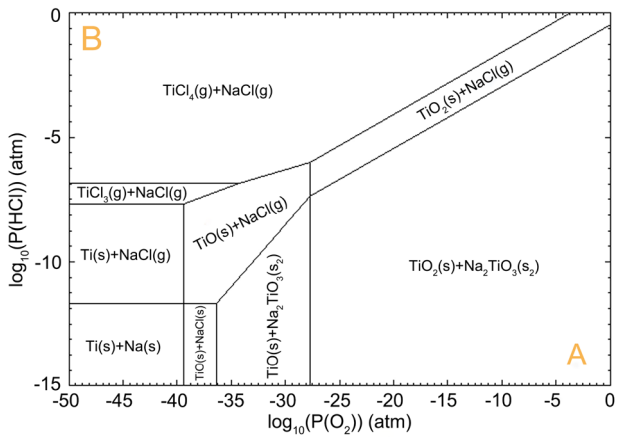

Fig. 8 The phase-stability diagram for Ti-Na-Cl-O-H at 600 °C calculated using FACTSAGE 7.2.

have been consumed. In this work, as shown in Fig. 3a, b, corrosion reactions occurred around solid NaCl on the surface of the sample at the initial time. With the deposition and consumption of NaCl, as shown in Fig. 3c–g, the morphology of NaCl does not present sharp edges but present rounded edges, which may attest to their progressive gas releasing. NaCl reacts with TiO_2 in presence of O_2 and H_2O, leading to the formation of Na-Ti oxides and HCl/Cl_2. The chemical reactions between NaCl, H_2O, and TiO_2 were as follows:

$$4NaCl_{(s)} + 2TiO_{2(s)} + O_{2(g)} \leftrightarrow 2Na_2TiO_{3(s)} + 2Cl_{2(g)} \quad (2)$$

$$4NaCl_{(s)} + 2TiO_{2(s)} + 2H_2O_{(g)} \leftrightarrow 2Na_2TiO_{3(s)} + 4HCl_{(g)} \quad (3)$$

$$4NaCl_{(g)} + 2TiO_{2(s)} + O_{2(g)} \leftrightarrow 2Na_2TiO_{3(s)} + 2Cl_{2(g)} \quad (4)$$

$$4NaCl_{(g)} + 2TiO_{2(s)} + 2H_2O_{(g)} \leftrightarrow 2Na_2TiO_{3(s)} + 4HCl_{(g)} \quad (5)$$

The cross-sectional morphologies showed that the oxide scale contained layered small pores and columnar voids that parallel to the oxide/metal interface. Cracks were found at the oxide/metal interface that lead to oxide scale decohesion on the substrate. A defected and delaminated oxide scale would increase the corrosion rate by affecting the diffusion conditions through the oxide scale[34]. The Cl_2/HCl was released then diffused inward through the destroyed oxide scale, reached the oxide/metal interface, reacted with the Ti substrate to form $TiCl_4$, and the Ti depletion of the metallic substrate that occurs in the direction of the lamella. Figure 9 shows an accumulation of chlorine at the oxide/metal interface, where no Na was present. This also demonstrated that $TiCl_4$ has formed at the oxide/metal interface. Fan et al.[18,19] and Ciszak et al.[21] also reported the presence of $TiCl_4$ after corrosion of Ti alloys in a solid NaCl deposit environment. $TiCl_4$ appears to have the highest-pressure vapor and in

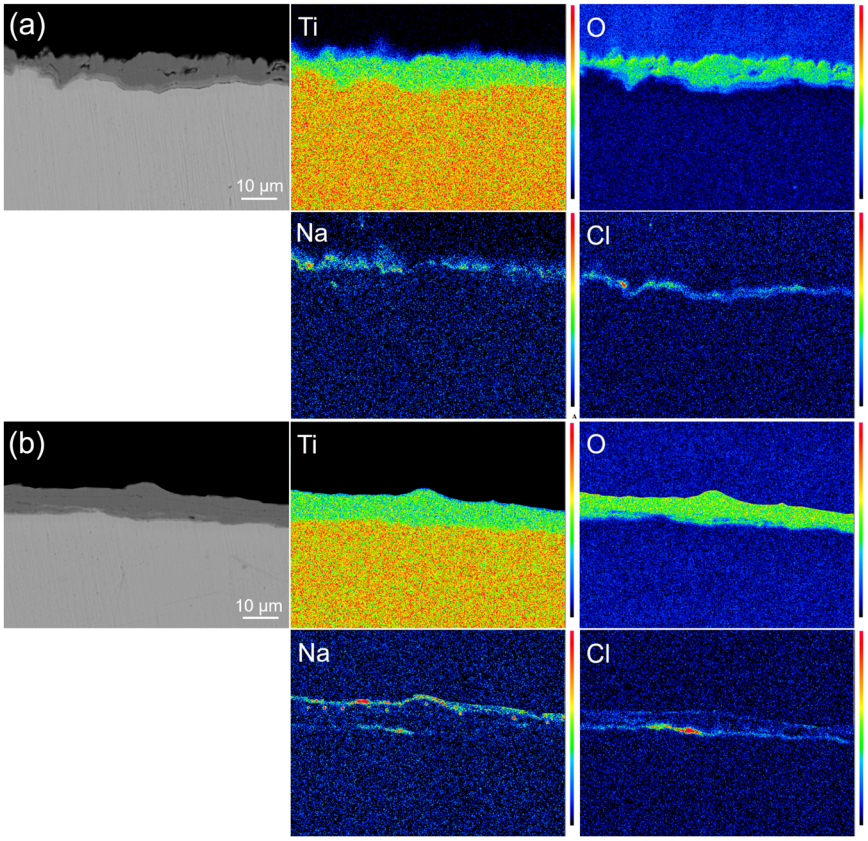

Fig. 9 EPMA elemental maps of corrosion products of pure Ti in continuous NaCl solution spraying at 600 °C for different times. a 5 h and **b** 20 h.

consequence, to be the most stable species of titanium chlorines in these experimental conditions. Therefore, $TiCl_4$ formed at the oxide/metal interface, where there is high partial pressure of Cl_2 and low partial pressure of O_2.

$$Ti_{(s)} + 2Cl_{2(g)} \leftrightarrow TiCl_{4(g)} \quad (6)$$

$$Ti_{(s)} + 4HCl_{(g)} \leftrightarrow TiCl_{4(g)} + 2H_{2(g)} \quad (7)$$

$TiCl_4$ will outward diffuse toward the atmosphere/oxide interface and will be oxidized when specific critical values of $P(O_2)$ will be reached. Chloride oxidation reactions are presented in Eqs. (8) and (9) below:

$$TiCl_{4(g)} + O_{2(g)} \leftrightarrow TiO_{2(s)} + 2Cl_{2(g)} \quad (8)$$

$$TiCl_{4(g)} + 2H_2O_{(g)} \leftrightarrow TiO_{2(s)} + 4HCl_{(g)} \quad (9)$$

TiO_2 continues to react with NaCl, O_2, and H_2O introduced by the environment according to Eqs. (4) and (5), releasing Cl_2/HCl that keep the mechanism of active oxidation up, these reactions happen circularly forming a repeated multi-layered oxide scale until the outer layer of Na_2TiO_3 was thick enough to prevent Cl diffusion through.

The standard Gibbs free-energy change (ΔG^o) of corrosion reactions calculated at 600 °C were presented in Table 1. Although the ΔG^o values of the Eqs. (2) and (3) were positive, as long as the partial pressure of the products (Cl_2 and HCl) on the right side of the formula was sufficiently low, chemical reactions (2) and (3) could still occur[1].

The formation of a repeated multi-layered oxide scale can also be understood with the help of the phase-stability diagram of Na-Ti-O-Cl-H calculated using FACTSAGE 7.2 at 600 °C (Fig. 8)[35–39]. The change in $P(O_2)$-P(HCl) combination corresponds to different thermodynamic conditions at different locations on the oxide scale. The phase-stability diagram suggests the phases which were stable or likely to form in the oxide scale. Layered small pores and columnar voids form a fresh reaction surface corresponding to area A in Fig. 8 (atmosphere/oxide interface with high oxygen partial pressure)[34]. Therefore, Na_2TiO_3 was the upper oxide layer and TiO_2 was the lower oxide layer. The bottom layer oxide corresponds to area B in Fig. 8 (oxide/metal interface with lower oxygen partial pressure). $TiCl_4$ formed at the oxide/metal interface. Depending on local $P(O_2)$ and P(HCl), when the $P(O_2)$ is high enough $TiCl_4$ will be oxidized to TiO_2. The corrosion conditions correspond to area A in Fig. 8 again, the inflow of the oxidizing atmosphere (NaCl, H_2O, and O_2) subsequently resulted in fresh

Table 1. The standard Gibbs free energy of the reactions at 600 °C.

Chemical reaction	ΔG^o (KJ mol^{-1})
$Ti + O_{2(g)} \leftrightarrow TiO_2$	−785.13
$Ti + 2H_2O_{(g)} \leftrightarrow TiO_2 + 2H_{2(g)}$	−385.82
$4NaCl_{(s)} + 2TiO_2 + O_{2(g)} \leftrightarrow 2Na_2TiO_3 + 2Cl_{2(g)}$	354.76
$4NaCl_{(s)} + 2TiO_2 + 2H_2O_{(g)} \leftrightarrow 2Na_2TiO_3 + 4HCl_{(g)}$	354.04
$4NaCl_{(g)} + 2TiO_2 + O_{2(g)} \leftrightarrow 2Na_2TiO_3 + 2Cl_{2(g)}$	−36.81
$4NaCl_{(g)} + 2TiO_2 + 2H_2O_{(g)} \leftrightarrow 2Na_2TiO_3 + 4HCl_{(g)}$	−37.53
$Ti + 2Cl_{2(g)} \leftrightarrow TiCl_{4(g)}$	−656.29
$Ti + 4HCl_{(g)} \leftrightarrow TiCl_{4(g)} + 2H_{2(g)}$	−256.26
$TiCl_{4(g)} + O_{2(g)} \leftrightarrow TiO_2 + 2Cl_{2(g)}$	−128.84
$TiCl_{4(g)} + 2H_2O_{(g)} \leftrightarrow TiO_2 + 4HCl_{(g)}$	−129.56

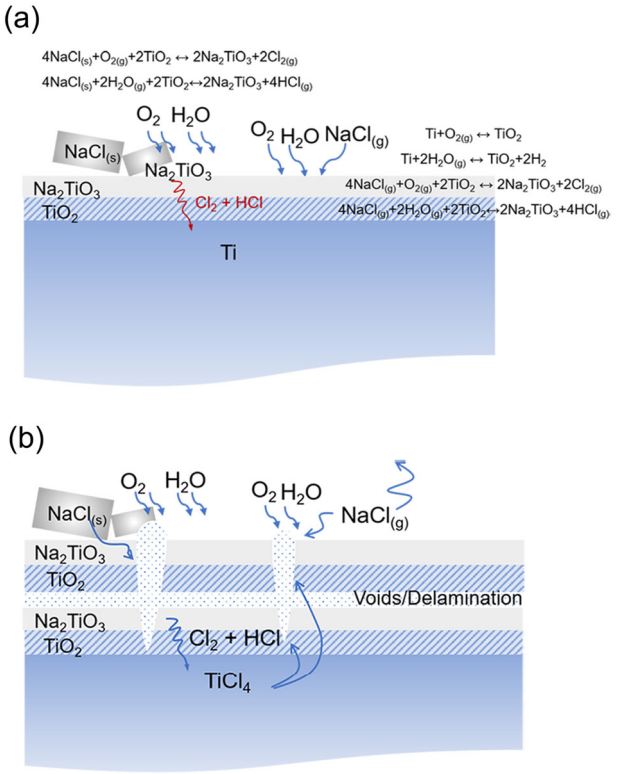

Fig. 10 Diagram of the corrosion mechanism of pure Ti in continuous NaCl solution spraying environment at 600 °C. **a** initial corrosion mechanism and **b** latter corrosion mechanism.

environmental conditions, these reactions will take place cyclically and form a repeated multi-layered oxide scale.

From this investigation, an oxidation process is schematically described in Fig. 10. The process started with the rapid deposition of NaCl over the sample surface. At the initial stage, oxygen partial pressure at the surface of the sample was higher, Ti oxides grew preferentially. when enough NaCl arrived in the system, NaCl reacted with TiO_2, a thin layer of Na_2TiO_3 was formed around NaCl particles. therefore, Na_2TiO_3 was the upper oxide layer and TiO_2 was the lower oxide layer. The reaction between gaseous NaCl and TiO_2 releasing Cl_2/HCl, Cl_2/HCl will diffuse inward and react with Ti forming volatile $TiCl_4$. The as-released $TiCl_4$ can be then partially released into the atmosphere, $TiCl_4$ will be oxidized into porous TiO_2 oxide (oxide scale with layered small pores and columnar voids pores) at the atmosphere/oxide interface. The inflow of the oxidizing atmosphere (NaCl, H_2O, and O_2) subsequently resulted in fresh environmental conditions, allowing for a subscale (upper subscale) to form upon the first Na_2TiO_3 and TiO_2 oxide scale (lower subscale), with subsequent growth of a repeat multi-layered oxide scale.

The corrosion mechanism of pure Ti[3,4] was studied under solid NaCl deposit film in water vapor at 600 °C in detail. Under a solid NaCl deposit film environment, a precoated solid NaCl film has been formed and the NaCl layer was thick at the beginning of corrosion, the partial pressure of O_2 and H_2O were relatively low at the interface of oxides/salt. Sufficient NaCl destroyed the TiO_2 scale to yield non-protective $Na_4Ti_5O_{12}$ and other volatile chloride, volatile chloride leading to the rapid establishment of an active oxidation process[23–26] and producing the porous structure of oxides[24].

Although the amount of deposition of NaCl in a continuous NaCl solution spraying environment (4.44 mg cm^{-2}) was slightly more than that in precoated NaCl condition (approximately 4 mg cm^{-2}) after 20 h of corrosion, the corrosion rate of the former was significantly lower than that of latter, which indicates that the corrosion mechanism should have been changed by differences in the environments. The corrosion products formed after 20 h corrosion in continuous NaCl solution spraying were also different from that under a solid NaCl deposit film environment. The reason for this should be the amount of transient NaCl deposition is very small, at a value of 0.0037 mg cm^{-2}, which is far less than the solid NaCl deposition amount[1]. The reactive amounts of NaCl, H_2O, and O_2 at the reaction interface of the oxides/salt under continuous NaCl solution spraying were different from those in the solid NaCl deposit film with H_2O + O_2. The NaCl deposit film formed by continuous NaCl solution spraying resulted in a process of gradual deposition, which also led to a gradual change in the corrosion reaction.

According to the above analysis, the relatively dense repeat delaminated TiO_2 reduced the corrosion rate. Although this compact Ti oxides scale could not inhibit active oxidation, it helped slow the corrosion rate. Most importantly, the deposition of solid NaCl in spraying was a gradual process, and the establishment of an active oxidation process was hindered by insufficient NaCl deposition. This high O_2 partial pressure environment also helped form a relatively compact Ti oxides layer. Therefore, although the continuous amount of NaCl deposited by the solution spray was more than that of the solid NaCl deposit (4 mg cm^{-2}), the mass gain of the pure Ti was less than that of the solid NaCl deposit in H_2O + O_2 at 600 °C.

In summary, the corrosion rate of the pure Ti under the NaCl solution spraying environment was significantly lower than that of the solid NaCl deposit environment. The oxide scale of pure Ti under the NaCl spraying environment is three repeat subscales composed of Na_2TiO_3 and TiO_2. NaCl spraying increase the volatilization of $TiCl_4$ towards the oxide/atmosphere interface as well as introduces pores and cracks, forming a fresh reactive surface and resulting in a duplicated and delaminated oxide scale.

Compared with a solid NaCl deposit film environment, in the present work, NaCl is deposited gradually with time, transient NaCl deposition is very small, the oxygen partial pressure is higher, and relatively dense duplicated and delaminated TiO_2 oxide scales have been formed. Both of these decrease the corrosion rate of the pure Ti under the NaCl solution spraying environment.

METHODS

Material preparation

The studied material was pure Ti courtesy of Alfa Aesar. Before the corrosion experiments, samples were cut into 15 mm × 10 mm × 2 mm pieces. According to previous studies, if the surface of the sample was too smooth, it was not conducive to NaCl deposition. Therefore, the samples were mechanically grounded with 800# SiC paper[18,19]. The samples were degreased and cleaned in acetone and ethanol solution using ultrasonic agitation.

Corrosion experiments

Corrosion experiments were isothermally performed in a vertical silica tube furnace (Ø = 35 mm). The 3.5% NaCl solution in the container was atomized into a NaCl spray by an ultrasonic mist device and then delivered to the furnace chamber. The temperature of the NaCl spray at the ultrasonic atomization nozzle was 70 °C, producing 30.8 vol.% water vapor. Oxygen took continuous NaCl spray into the furnace, and the flow rate was 310 mL min^{-1}. During the 20 h experiment, salt was continuously deposited on the sample surface at 600 °C.

The two kinds of comparison experiments were as follows: one was performed without NaCl[19] (the samples were placed into a furnace at a fixed temperature 600 °C and H_2O + O_2 atmosphere, H_2O 30.8 % and O_2 310 mL min^{-1}); the other experiment was a solid NaCl deposited under H_2O + O_2[19] (a solid NaCl deposit film was precoated on the sample surface, and then the samples were placed into a furnace with an H_2O + O_2 atmosphere, the amount of deposited NaCl was approximately 4 ± 0.2 mg cm^{-2}, H_2O 30.8% and O_2 310 mL min^{-1}).

The weight of samples was recorded before and after corrosion using a five-decimal Sartorius balance. Each experiment was performed with more than four samples at least three times to confirm its accuracy.

Characterization

According to Cao's work, the total deposited NaCl amount has been calculated by experimental results: there is the assumption that the deposition rate of NaCl particles in solution is constant, and the maximum calculated amount of NaCl deposited on the samples will be 4.44 mg cm^{-2} after 20 h[1].

After corrosion, the samples were analyzed. The surface morphologies of the corrosion products were performed by an FEI INSPECT F50 scanning electron microscopy (SEM). The phase composition of the corrosion products was determined by X'Pert PRO X-ray diffraction (XRD) with Cu *Kα* radiation ($\lambda = 0.1541$ nm). The measuring range is $20° < 2\theta < 90°$.

The samples were embedded in epoxy resin, grounded with 5000# SiC paper, and finally polished with diamond paste for cross-sectional observation by SEM. Cross-sectional characterization of the samples was performed by an FEI INSPECT F50 SEM. The cross-sectional elemental distribution of the corrosion products was analyzed by 1610-electron probe microanalysis (EPMA).

The microstructure of selected features was investigated by the cross-sections of TEM prepared using focused-ion beam (FIB) FEI Helios G4. The instrument was operated in high vacuum mode at 30 kV, with varying beam currents (30 pA-15 nA) throughout the lift-out procedure. And the lamella sample was fixed to the Cu-grid using the micromanipulator. Finally, the lamella sample was thinned down to a thickness of around 100 nm. A cross-section lamella sample was cut from the outer layer oxide to the substrate.

For further understanding of the corrosion of substrate, a fine characterization was performed. TEM investigations of TEM lamellas obtained by FIB were performed using JEM 2100F operated at 200 kV. The resolution of the instrument is 0.19 nm. A systematic analysis of the microstructure and crystalline structure of the different compounds and composition was performed by low- and high-magnification TEM images, STEM-EDS, and SAED.

DATA AVAILABILITY

The data that support the findings of this study are available from the corresponding author upon reasonable request.

Received: 28 March 2022; Accepted: 19 May 2022;
Published online: 01 July 2022

REFERENCES

1. Cao, M. et al. Studies on the corrosion behavior of Fe-20Cr alloy in NaCl solution spray at 600 °C. *Corros. Sci.* **133**, 165–177 (2018).
2. Sun, W. et al. Studies on corrosion behavior of a single-crystal superalloy and its sputtered nanocrystalline coatings with solid NaCl deposit in O_2 + 38 vol.% H_2O environment at 700 °C. *Corros. Sci.* **161**, 108187 (2019).
3. Fan, L. et al. Effects of pre-oxidation on the corrosion behavior of pure Ti under coexistence of solid NaCl deposit and humid oxygen at 600 °C: the diffusion of chlorine. *Sci. Rep.* **10**, 16291 (2020).
4. Fan, L. et al. Corrosion behavior of pure Ti under a solid NaCl deposit in a wet oxygen flow at 600 °C. *Metals* **6**, 72–83 (2016).
5. Shu, Y., Wang, F. & Wu, W. Synergestic effect of NaCl and water vapor on the corrosion of 1Cr11Ni2W2MoV steel at 500-700 °C. *Oxid. Met.* **51**, 97–110 (1999).
6. Shu, Y., Wang, F. & Wu, W. Corrosion behavior of pure Cr with a solid NaCl deposit in O_2 plus water vapor. *Oxid. Met.* **54**, 457–471 (2000).
7. Wang, F. & Shu, Y. Influence of Cr content on the corrosion of Fe-Cr alloys: the synergistic effect of NaCl and water vapor. *Oxid. Met.* **59**, 201–214 (2003).
8. Wang, F., Geng, S. & Zhu, S. Corrosion behavior of a sputtered K38G nanocrystalline coating with a solid NaCl deposit in wet oxygen at 600 to 700 °C. *Oxid. Met.* **58**, 185–195 (2002).
9. Wang, C., Jiang, F. & Wang, F. Corrosion inhibition of 304 stainless steel by nano-sized Ti/Silicone coatings in an environment containing NaCl and water vapor at 400–600 °C. *Oxid. Met.* **62**, 1–13 (2003).
10. Liu, L., Li, Y., Zeng, C. & Wang, F. Electrochemical impedance spectroscopy (EIS) studies of the corrosion of pure Fe and Cr at 600 °C under solid NaCl deposit in water vapor. *Electrochim. Acta* **51**, 4736–4743 (2006).
11. Liu, L., Li, Y. & Wang, F. Corrosion behavior of metals or alloys with a solid NaCl deposit in wet oxygen at medium temperature. *Sci. China Technol. Sci.* **55**, 369–376 (2012).
12. Tang, Y., Liu, L., Li, Y. & Wang, F. The electrochemical corrosion mechanisms of pure Cr with NaCl deposit in water vapor at 600 °C. *J. Electrochem. Soc.* **158**, C237–C241 (2011).
13. Tang, Y., Liu, L., Li, Y. & Wang, F. Evidence for the occurrence of electrochemical reactions and their interaction with chemical reactions during the corrosion of pure Fe with solid NaCl deposit in water vapor at 600 °C. *Electrochem. Commun.* **12**, 191–193 (2010).
14. Li, Y., Niu, Y. & Wu, W. Accelerated corrosion of pure Fe, Ni, Cr and several Fe-based alloys induced by $ZnCl_2$-KCl at 450 °C in oxidizing environment. *Mater. Sci. Eng.* **A345**, 64–71 (2003).
15. Gao, X., Zeng, W., Zhang, S. & Wang, Q. A study of epitaxial growth behaviors of equiaxed alpha phase at different cooling rates in near alpha titanium alloy. *Acta Mater.* **122**, 298–309 (2017).
16. Peng, W., Zeng, W., Wang, Q. & Yu, H. Characterization of high-temperature deformation behavior of as-cast Ti60 titanium alloy using processing map. *Mater. Sci. Eng., A* **571**, 116–122 (2013).
17. Williams, J. C. & Starke, E. A. Progress in structural materials for aerospace systems. *Acta Mater.* **51**, 5775–5799 (2003).
18. Fan, L. et al. Corrosion behavior of Ti60 alloy under a solid NaCl deposit in wet oxygen flow at 600 °C. *Sci. Rep.* **6**, 29019 (2016).
19. Fan, L. et al. Effect of streaming water vapor on the corrosion behavior of Ti60 alloy under a solid NaCl deposit in water vapor at 600 °C. *Corros. Sci.* **160**, 108177 (2019).
20. Ciszak, C., Popa, I., Brossard, J. M., Monceau, D. & Chevalier, S. NaCl-induced high-temperature corrosion of β21S Ti alloy. *Oxid. Met.* **87**, 729–740 (2017).
21. Ciszak, C., Popa, I., Brossard, J. M., Monceau, D. & Chevalier, S. NaCl induced corrosion of Ti-6Al-4V alloy at high temperature. *Corros. Sci.* **110**, 91–104 (2016).
22. Ciszak, C. et al. Degradation mechanism of Ti-6Al-2Sn-4Zr-2Mo-Si alloy exposed to solid NaCl deposit at high temperature. *Corros. Sci.* **172**, 108611 (2020).
23. Shinata, Y. Accelerated oxidation rate of chromium induced by sodium chloride. *Oxid. Met.* **27**, 315–332 (1987).
24. Grabke, H. J., Reese, E. & Spiegel, M. The effects of chlorides hydrogen chloride, and sulfur dioxide in the oxidation of steels below deposits. *Corros. Sci.* **37**, 1023–1043 (1995).
25. Nielsen, H. P., Frandsen, F. J. & Dam-Johansen, K. Lab-scale investigations of hightemperature corrosion phenomena in straw-fired boilers. *Energy Fuel* **13**, 1114–1121 (1999).
26. Nielsen, H. P., Frandsen, F. J., Dam-Johansen, K. & Baxter, L. L. The implications of chlorine-associated corrosion on the operation of biomass-fired boilers. *Prog. Energy Combust.* **26**, 283–298 (2000).
27. Dumas, P. & John, C. S. NaCl-induced accelerated oxidation of a titanium alloy. *Oxid. Met.* **10**, 127–134 (1976).
28. Xiong, Y., Zhu, S. & Wang, F. The oxidation behavior and mechanical performance of Ti60 alloy with enamel coating. *Surf. Coat. Technol.* **190**, 195–199 (2005).
29. Guleryuz, H. & Cimenoglu, H. Oxidation of Ti-6Al-4V alloy. *J. Alloy. Compd.* **472**, 241–246 (2009).
30. Guleryuz, H. & Cimenoglu, H. Surface modification of a Ti-6Al-4V alloy by thermal oxidation. *Surf. Coat. Technol.* **192**, 164–170 (2005).
31. Poquillon, D., Armand, C. & Huez, J. Oxidation and oxygen diffusion in Ti-6Al-4V alloy: improving measurements during sims analysis by rotating the sample. *Oxid. Met.* **79**, 249–259 (2013).
32. Xiong, Y., Zhu, S. & Wang, F. Synergistic corrosion behavior of coated Ti60 alloys with NaCl deposit in moist air at elevated temperature. *Corros. Sci.* **50**, 15–22 (2008).
33. Jonsson, T., Folkeson, N., Svensson, J. E., Johansson, L. G. & Halvarsson, M. An ESEM in situ investigation of initial stages of the KCl induced high temperature corrosion of a Fe-2.25Cr-1Mo steel at 400 °C. *Corros. Sci.* **53**, 2233–2246 (2011).
34. Persdotter, A. et al. Oxidation of Fe-2.25Cr-1Mo in presence of KCl(s) at 400 °C - crack formation and its influence on oxidation kinetics. *Corros. Sci.* **163**, 108234 (2020).
35. Okoro, S. C., Kiamehr, S., Montgomery, M., Frandsen, F. J. & Pantleon, K. Effect of flue gas composition on deposit induced high temperature corrosion under laboratory conditions mimicking biomass firing. Part I: Exposures in oxidizing and chlorinating atmospheres. *Mater. Corros.* **68**, 499–514 (2017).
36. Metsajoki, J., Huttunen-Saarivirta, E. & Lepisto, T. Elevated-temperature corrosion of uncoated and aluminized 9-12% Cr boiler steels beneath KCl deposit. *Fuel* **133**, 173–181 (2014).
37. Zhang, S. et al. Chloride- and sulphate-induced hot corrosion mechanism of super austenitic stainless steel S31254 under dry gas environment. *Corros. Sci.* **163**, 108295 (2020).
38. Chandra, K., Dorfel, I., Wollschlager, N. & Kranzmann, A. Microstructural investigation using advanced TEM techniques of inner oxide layers formed on T92 steel in oxyfuel environment. *Corros. Sci.* **148**, 94–109 (2019).
39. Chandra, K., Kranzmann, A., Saliwan Neumann, R. & Rizzo, F. Comparative study on high temperature oxidation of T92 steel in dry and wet oxyfuel environments. *Oxid. Met.* **84**, 463–490 (2015).

ACKNOWLEDGEMENTS

The investigation was supported by the National Natural Science Foundation of China under Contract No. U20B2026 and No. 51871049.

AUTHOR CONTRIBUTIONS

R. Li (first author): performed the experiments, analyzed experimental data, and wrote the manuscript. L.L. (corresponding author): designed the research, wrote and revised the paper, and provided financial support. Y.C.: discussed the experimental scheme and maintained the equipment used in this work. R. Liu: discussed the experimental data. F.W.: provided workplace and experimental equipment storage sites.

COMPETING INTERESTS

The authors declare no competing interests.

ADDITIONAL INFORMATION

Supplementary information The online version contains supplementary material available at https://doi.org/10.1038/s41529-022-00257-x.

Correspondence and requests for materials should be addressed to Li Liu.